Protic ammonium bio-based ionic liquid crystal lubricants

M.D. Avilés, R. Pamies, J. Sanes, J. Arias-Pardilla, F.J. Carrión, M.D. Bermúdez [*]

Grupo de Ciencia de Materiales e Ingeniería Metalúrgica. Universidad Politécnica de Cartagena, Campus de La Muralla Del Mar. 30202, Cartagena, Spain

ARTICLE INFO

ABSTRACT

Bis(2-hydroxyethyl) ammonium stearate (DES) protic ionic liquid crystal (PILC) has been added in 1 wt% and 2 wt% proportion to di-bis(2-hydroxyethyl) ammonium succinate (DSU) protic ionic liquid (PIL) to obtain (DSU+1%DES) and (DSU+2%DES) lubricant blends. The new blends are non-Newtonian fluids with liquid crystalline domains. Addition of (DES) PILC to (DSU) PIL reduces running-in friction coefficient in more than 70% and prevents surface damage, decreasing wear rate in more than one order of magnitude. Optical profilometry, optical and scanning electron microscopy (SEM), energy dispersive (EDX) and X-ray photoelectron spectroscopy (XPS) have been used to analyze surfaces after the tribological tests.

1. Introduction

After the first 20 years [1] of increasingly active research on ionic liquid lubricants [2–6], there exists a pronounced interest in the development of bio-based lubricants and lubricant additives [7–14] containing anions derived from natural-source carboxylic acids. Short alkyl chain protic ammonium carboxylate ionic liquids have shown their outstanding performance both as neat lubricants and as additives [15–17]. A triprotic ammonium succinate ionic liquid presents excellent ability to give ultralow friction as additive in water lubrication of sapphire-stainless steel [17]. Similarly, diprotic ammonium adipate ionic liquid showed ultralow friction and absence of wear as neat lubricant and excellent friction and wear reduction behavior as 1 wt% additive in PAO 6 [18].

Recent developments have been focused on the use of fatty acid derived ionic liquids [19–30]. Protic ammonium carboxylate salts with long alkyl chain anions such as stearate, palmitate, oleate, etc., present a mesomorphic nature and their phase behavior has been recently characterized [25]. The long alkyl chains present in these anions promote the formation of mesophases, with liquid crystalline properties [15,16, 25–30].

Water-based lubricants are a renewable resource, although currently used additives such as halogenated species and volatile organic compounds can be toxic or give rise to hazardous residues. Many efforts are currently directed towards the development of suitable additives [31]. Short alkyl chain protic ammonium ionic liquids are soluble in water and give rise to a thin boundary layer upon water evaporation, which results in ultralow friction and negligible wear [17,30]. In contrast, long

alkyl chain fatty acid-derived ionic liquids are not always soluble or stable in water. Moreover, under severe sliding conditions, water evaporation increases friction and wear due to the precipitation of the solid ionic liquid phase at the sliding contact.

Previous studies [30] have shown that 1 wt% addition of bis (2-hydroxyethyl) ammonium stearate (DES) PILC to water reduces friction coefficient in AISI 316L steel-sapphire lubrication from approximately 0.4 to 0.12. However, water evaporation takes place under sliding conditions, thus increasing friction coefficient to around 0.3 due to the presence of solid DES at the steel-sapphire interface. To avoid this kind of aqueous lubricant failure, the applied strategy has been the substitution of water by an ionic liquid which can act as base lubricant for another ionic liquid additive. The only precedent, very recently reported [28], is the excellent tribological performance of a spin-coated thin film deposited from a citrate protic ionic liquid (PIL) containing a palmitate protic ionic liquid crystal (PILC) as additive.

The advantages of using ionic liquid blends are mainly focused on the possibility of tailoring their properties, such as lowering their melting points. In this particular case, the main purpose was to combine two environmentally friendly thermally stable non-corrosive ionic liquids with the advantage of using a liquid crystalline ionic liquid below its melting point and to avoid the low thermal stability and corrosiveness of water.

In the present work, we have selected the PILC (DES) as additive in di-bis(2-hydroxyethyl) ammonium succinate (DSU) isotropic PIL as base lubricant. The main purpose was to develop lubricant blends with the ability to reduce the running-in friction coefficient and the wear rate of neat DSU under severe contact conditions.

---

2. Materials and methods

Ionic liquid DSU (Fig. 1a) and ionic liquid crystal DES (Fig. 1b) were obtained from the reaction between 2-hydroxyethylamine and succinic or stearic acid, respectively [25,32]. (DSU+1 wt%DES) and (DSU+2 wt%DES) blends (from now on DSU+1%DES and DSU+2%DES, respectively) were ultrasonicated for 30 min to ensure a homogeneous dispersion before their use as lubricants in the tribological tests.

Raman microscopy spectra were recorded with a WiTec UHTS 300 (WITec GmbH, Ulm, Germany) equipment, using a 532 nm laser.

Differential scanning calorimetry (DSC) analysis was obtained with a DSC 822e (Mettler Toledo, USA) under N_2 (50 mL/min) flow, at a heating rate of 10 °C/min. After a first heating cycle from 0 °C to 150 °C, samples were cooled from 150 to 0 °C, before recording the second 0 °C to 150 °C heating cycle.

Thermogravimetric analysis (TGA) was performed with a TGA 1HT (Mettler Toledo, USA) under an oxygen atmosphere using a 10 °C/min heating rate, in the temperature range from 30 to 600 °C.

Images of mesomorphic transitions were obtained between cross polarizers using a BH2 Olympus microscope while heating the samples in a Mettler FP82 heating stage, connected to a Mettler FP90 control unit.

Rheological behavior was determined by a rotational rheometer (AR-G2; TA instruments, New Castle, Delaware, USA). Viscosity variation with shear rate was measured at 25 °C.

Tribological tests were carried out under ambient conditions (Temperature: 25±1 °C; Relative Humidity: 40%) in a pin-on-disk tribometer (ISC 200 PC, Implant Corporation, USA). AISI 316L stainless steel disks of 25 mm diameter and 5 mm thickness [Ra<0.15 μm; HV 200; Young's modulus 197 GPa; Poisson's ratio 0.27] were tested against sapphire balls (Goodfellow Cambridge Ltd.UK) [Al_2O_3; 99.9%; HV 2750; Young's modulus 445 GPa; Poisson's ratio 0.24]. These immersion tests were developed under a load of 0.98 N (mean contact pressure 1.30 GPa; maximum contact pressure 1.95 GPa), at a speed of 0.10 m/s, a sliding radius of 9.0 mm and a sliding distance of 1500 m, with an added lubricant volume of 0.2 mL. All tests were repeated at least three times under the same conditions. Surfaces were cleaned with n-hexane and dried in hot air.

Wear measurements, cross-section profiles and 3D surface topography for stainless steel disks were determined with a Talysurf CLI optical profiler. SEM micrographs and EDX element maps were obtained using a Hitachi S3500 N electron microscope.

3. Results and discussion

3.1. Lubricants characterization and rheological behavior

Raman spectra for neat DSU and DES are shown in Fig. 2a. Both DSU and DES show very strong absorptions close to 3000 cm^{-1} and weak peaks in the 1400-1500 cm^{-1} region. DSU peaks at 2975 cm^{-1} (very strong) and 2940 cm^{-1} (very strong shoulder) correspond to ν(C-H) stretching; absorptions at 1470 (weak) and 1428 (weak) cm^{-1} are characteristic of δ(C-H) deformation modes. The Raman spectrum of neat DES show ν(C-H) stretching bands at 2889 (very strong) cm^{-1} and
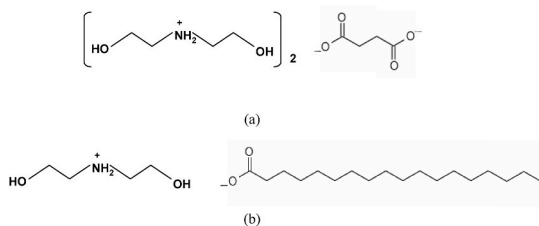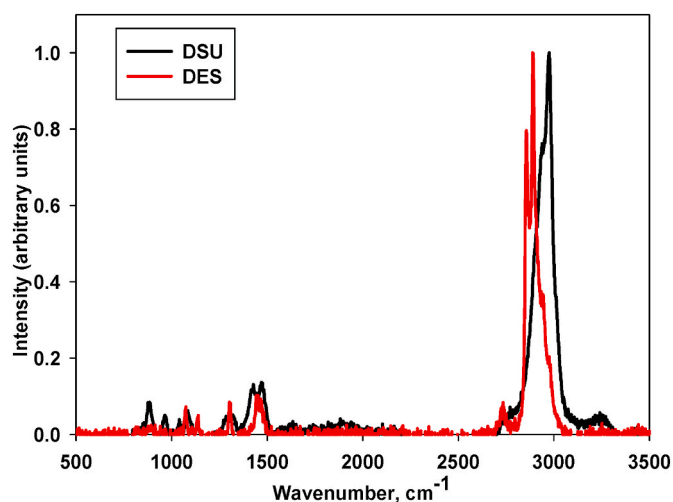

Fig. 2a. Raman microscopy spectra for neat DSU and neat DES.

2856 (very strong) cm^{-1}, and a δ(C-H) deformation band at 1443 (weak). A very weak peak at 885 cm^{-1}, assignable to (CH_2) rocking mode is only observed for the short chain DSU [33]. Raman spectra of (DSU + DES) blends (Fig. 2b) contain only the peaks of DSU, due to the low concentration of DES added to DSU.

As can be observed in the TGA thermograms shown in Fig. 3, both neat DSU and blends show three thermal degradation steps, at 180, 230 and 326 °C, to reach a nearly complete weight loss at 597 °C. The weight loss onset temperature is displaced from 116.2 °C for neat DSU (attributed to the loss of water), to higher temperatures by the addition of DES: 134.8 °C for (DSU+1%DES), and 136.2 °C for (DSU+2%DES), respectively. This higher thermal stability of the blends is maintained up to 350 °C, and could contribute to their better tribological results.

DSC phase transitions temperatures observed for the mesomorphic DES phase (Fig. 4) are similar for both (DSU + DES) blends: 50.3 °C for (DSU+1%DES) and 50.6 °C for (DSU+2%DES), and lower than that of neat DES (53.3 °C). The intensity of the peaks is weak for (DSU+2%DES) and very weak for (DSU+1%DES), as corresponds to the low concentration of DES.

Polarized optical microscopy image for (DSU+1%DES) (Fig. 5a) shows mesomorphic droplet domains in an isotropic (black) background. Increasing DES concentration to 2 wt% induces the formation of oily streaks at the beginning of the transition (Fig. 5b), which transforms into an isotropic fluid phase with maltese crosses at the edges (magnified detail in Fig. 5c), characteristic of a smectic liquid crystalline phase [25]. The lubricant blends used in the present study are formed by an isotropic fluid (DSU) and a liquid crystal fluid (DES). The birefringence images shown in Fig. 5 correspond to the transformation of DES to a fluid liquid crystalline phase. These phase transitions depend on temperature, as shown in Fig. 4. After the liquid crystal transition has finished, the blends behave again as isotropic fluids.

Neat DSU shows the rheological behavior of a Newtonian fluid (Fig. 6), with a constant viscosity of 177 mPa s in the entire range of shear rates. This is in agreement with other short alkyl chain protic ionic liquids [15,16].

The non-Newtonian nature of DES and other fatty acid derived ionic liquid crystals has been previously described [25]. The mesomorphic nature of fatty acid derived protic ionic liquid crystals, with more than ten carbon atoms in the carboxylate anion, such as in the case of DES, induces a non-Newtonian rheology [15,16], associated to the stronger molecular interactions in the liquid crystalline phases, which require high shear to start flowing.

The new (DSU+1%DES) and (DSU+2%DES) blends are highly viscous non-Newtonian fluids (Fig. 6). The addition of DES increases initial low shear viscosity from 177 mPa s to approximately 800 mPa s,

Fig. 1. a) Di-[bis(2-hydroxyethyl)ammonium]succinate base lubricant; b) Bis (2-hydroxyethyl) ammonium stearate additive.

to reach asymptotic behavior, with constant viscosity values around 500 mPa s under increasing shear rate values. This rheological behavior is attributed to the presence of highly ordered DES mesophases in the blends, as discussed above for DSC (Fig. 4) and by light-polarized optical microscopy (Fig. 5) results. The very high viscosity of the blends with respect to neat DSU could anticipate a higher load-carrying ability under tribological conditions.

Table 1 shows contact angle values for lubricant blends and neat DSU on AISI 316L stainless steel surface. Addition of DES reduces the initial contact angles of DSU on stainless steel surface. This result could be interpreted in terms of a stronger interaction of the lubricant molecules with the steel surface under static conditions. Although contact angles are determined under static conditions, these stronger interactions could also facilitate the formation of boundary layers. After 5 min, contact angles for the blends are also lower but differences are small, particularly taking into account deviation values.

3.2. Tribological performance

3.2.1. Friction coefficients

As shown in Fig. 7 and Table 2, the main advantage of the addition of DES to DSU is the sharp reduction in the running-in friction coefficient, from 0.22 for neat DSU to 0.10 for (DSU+2%DES) and to 0.06 for (DSU+1%DES).

The remarkable improvement reached when using the blends is attributed to the formation, from the start of the sliding, of an ordered effective lubricant layer due to the longer lateral chain present in DES additive. Recent results on the influence of water content on the tribological performance of highly hygroscopic ionic liquids [34] have shown a reduction of the running-in friction coefficients with the reduction in water content. In the present case, the observed displacement of the onset temperature to higher values for the blends with respect to neat DSU (Fig. 3), could be attributed to a higher water content in DSU.

The lower initial friction coefficient for (DSU+1%DES) with respect to (DSU+2%DES) could be due to its slightly lower viscosity and to a better dispersion of the lower concentration of DES in DSU. Moreover, increasing DES concentration does not significantly improve steady-state lubrication.

After a sliding distance of 100 m, a friction coefficient of 0.07 is reached for both (DSU+1%DES) and (DSU+2%DES) blends. At 400 m, the three lubricants present similar friction coefficient values, close to 0.10. From this point to the end of the tests, after a sliding distance of 1500 m, friction coefficients are similar, in the range of 0.11–0.12, for all
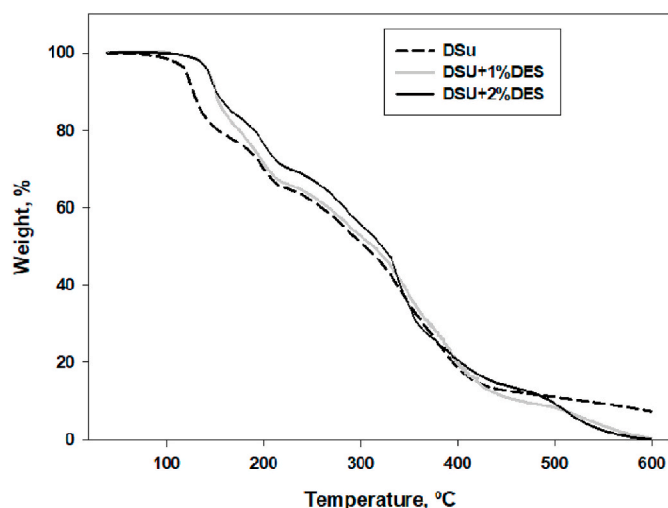
Fig. 3. TGA thermograms for the three lubricants.

lubricants (Table 2; Fig. 7). Average friction coefficient values for the whole sliding period (Table 2) are very similar, 0.1 for DSU and (DSU+1%DES), and closer to 0.09 for (DSU+2%DES). In contrast, when DES was used as additive in water under the same conditions, the average friction coefficient was 0.12, but with an increase to 0.20 as a consequence of water evaporation and precipitation of solid DES at the interface after a sliding distance of 1340 m [30].

The results described here confirm that the substitution of water by DSU as base lubricant in (DSU + DES) blends, maintains friction coefficients lower than 0.12, and prevents high running-in friction and transitions to higher friction coefficients due to water evaporation [30], which take place in lubrication with (Water + DES).

3.2.2. Wear rates and surface analysis

Surface topography and cross section profiles of the wear scars on steel disks after lubrication with DSU, (DSU+1%DES) and (DSU+2% DES) are shown in Figs. 8 and 9a, respectively.

The scheme presented in Fig. 9b shows the cross section areas which have been measured to calculate wear rates (Table 3). Wear rates can be calculated taking into account only the material volume loss (calculated from $[A_3–(A_1+A_2)]$), or as the total surface damage, considering both material loss below the surface line and plastic deformation material accumulated on the scar edges (calculated from $[A_1+A_2+A_3]$).
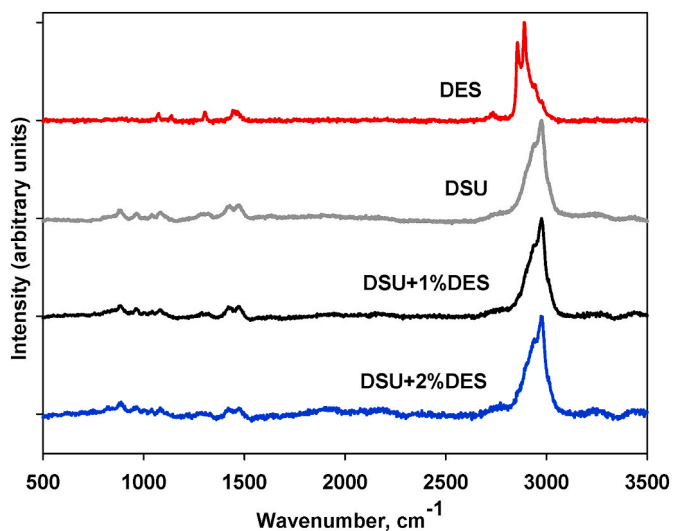
Fig. 2b. Raman microscopy spectra of lubricant blends compared with those of neat DSU and DES.
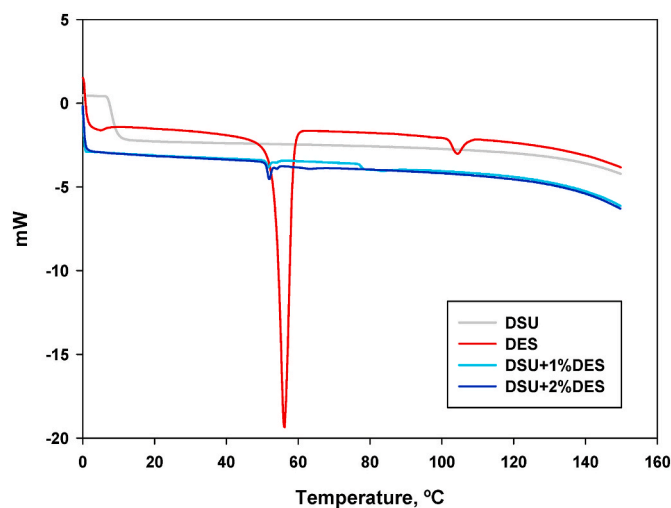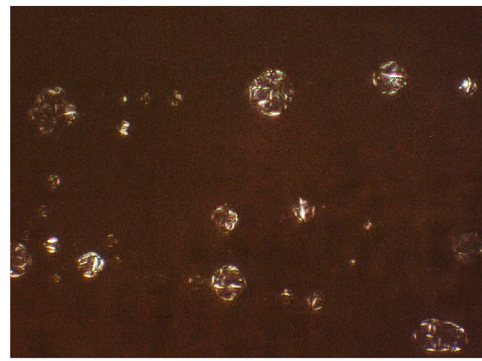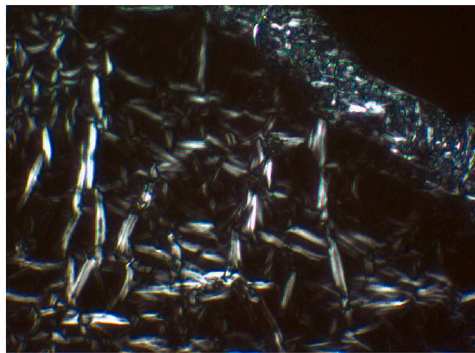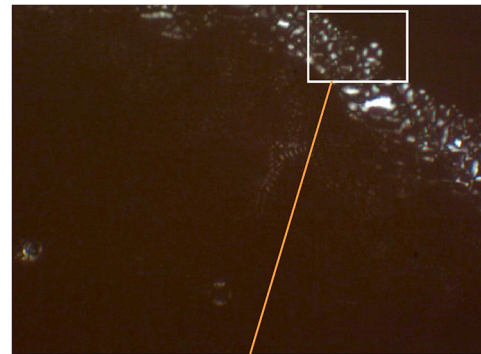
Fig. 4. DSC curves for neat DSU, neat DES and for (DES+1%DES) and (DSU+2%DES) blends.
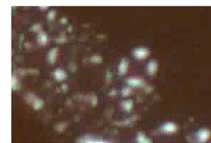
(a)

(b)

(c)

Fig. 5. Polarized optical micrographs of mesophases: a) (DSU+1%DES); b) (DSU+2%DES) at the onset, and c) at the end of the mesomorphic transformation, and detail of maltese crosses.
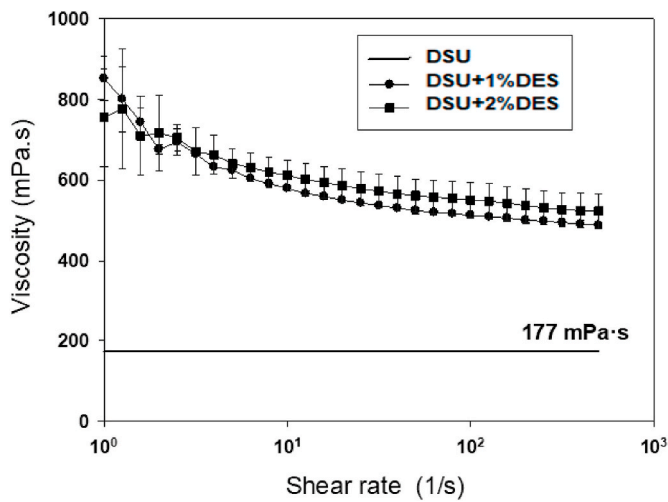

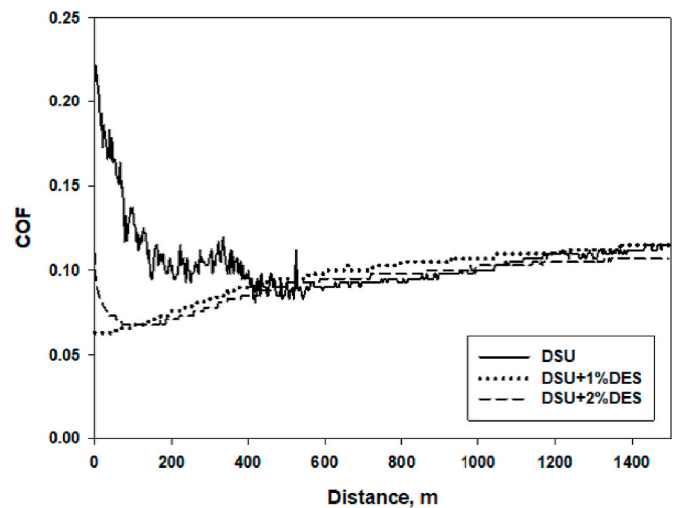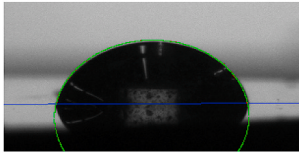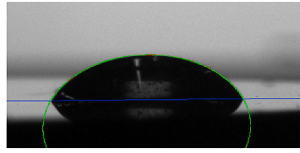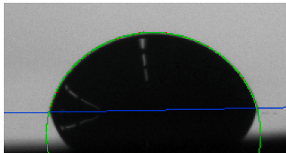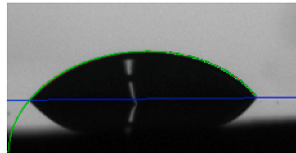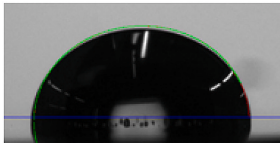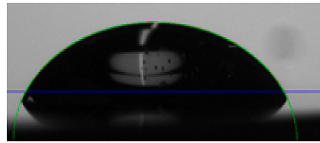**Fig. 6.** Viscosity vs shear rate for the three lubricants at 25 °C.

Fig. 7. Coefficient of friction (COF) vs sliding distance for the three lubricants.

Table 1
Contact angles.

	Contact angles on stainless steel	
	Initial	After 5 min
DSU+1%DES	74.7 ± 6.7	52.3 ± 3.2
DSU + 2%DES	**75.1 ± 0.8**	**49.1 ± 3.6**
DSU	**89.9 ± 1.9**	**56.9 ± 3.0**

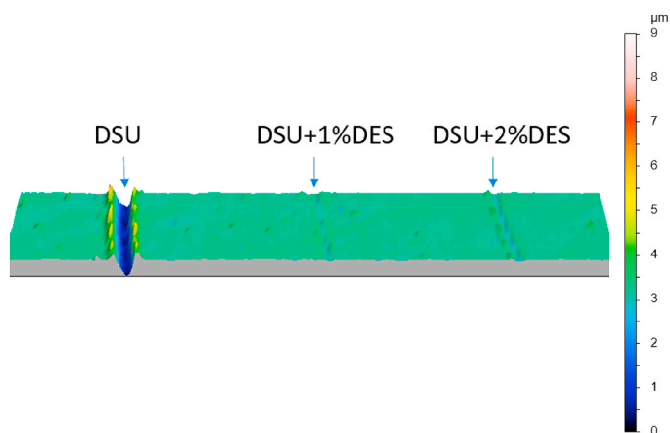**Fig. 8.** Surface topography of wear scars on AISI 316L steel disks after lubrication with neat DSU and (DSU+1%DES) and (DSU+2%DES) blends.

Fig. 9. a) Cross section profiles of wear tracks on AISI 316L disks and b) scheme showing cross section areas used for the calculation of wear rates values shown in Table 3.

Table 2
Evolution of coefficient of friction with sliding distance (standard deviation ≤ 0.010).

Lubricant	Coefficient of Friction			
	Initial	400 m	1500 m	Average (0–1500 m) (standard deviation)
DSU	0.22	0.10	0.12	0.098 (0.008)
DSU+1%DES	0.06	0.10	0.12	0.099 (0.007)
DSU+2%DES	0.10	0.09	0.11	0.094 (0.009)

The anti-wear performance of (DSU + DES) blends is clearly pointed out by the wear rate reduction with respect to DSU, which is close to 95% for (DSU+2%DES) and higher than 95% for (DSU+1%DES) (Fig. 9a and Table 3). Wear rates are also one order of magnitude lower for both (DSU + DES) blends than that described [24] for (Water+1%DES) lubricant under the same sliding conditions.

The very high friction coefficient obtained for DSU during the first 400 m (Table 2) is in agreement with the severe wear rate and surface damage (Table 3). Several factors could contribute to this results. The absence of ordered mesophases, the low viscosity and the short alkyl chain of the succinate anion could reduce the ability of DSU molecules to form adsorbed layers to separate the sliding surfaces. Contact angles have shown a weaker initial affinity of DSU for steel surface. TGA of neat DSU shows a higher weight loss at low temperature than that observed for (DSU + DES) blends (Fig. 3). This could be due to the presence of

(a)

(b)

(c)

(d)

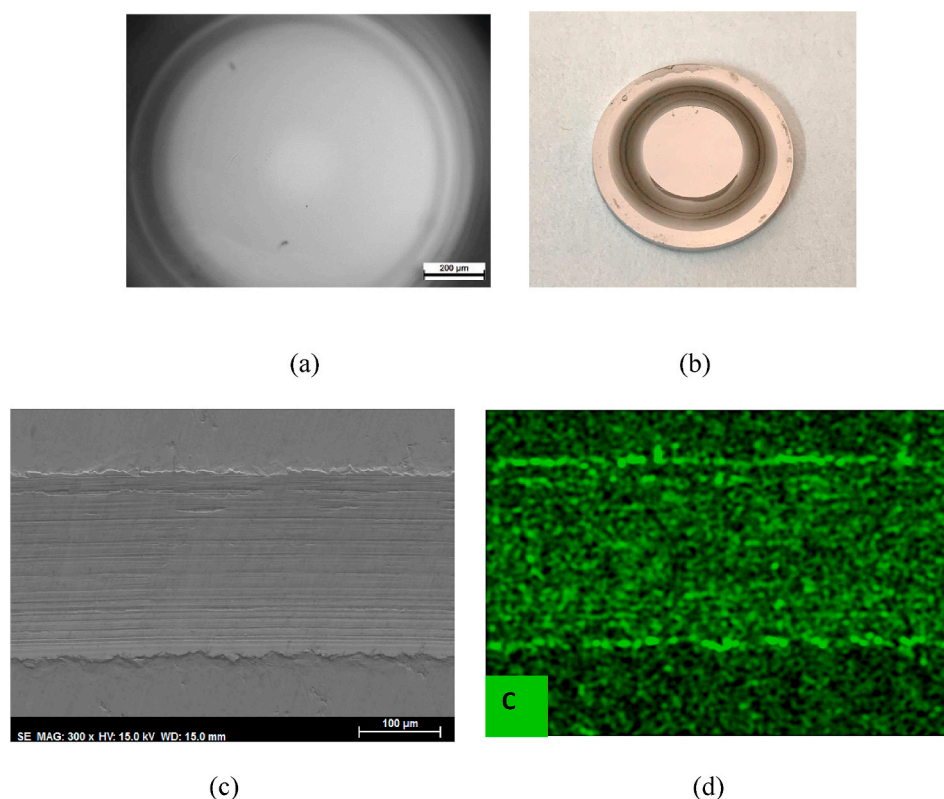**Fig. 10.** Lubrication with DSU: a) Sapphire ball; b) Photograph of the AISI 316L disk after the test; c) SEM micrograph of wear track on AISI 316L steel disk; d) EDX carbon element map.

Table 3
Wear rates calculated from cross section profiles shown in Fig. 13.

Lubricant	Wear rate ($mm^3 \cdot N^{-1} \cdot m^{-1}$)	
	Calculated from [A_3-(A_1+A_2)]	Calculated from [A_1+A_2+A_3]
DSU	1.40E-05 (7.86E-07)	1.79E-05 (9.00E-07)
DSU+1%DES	7.46E-07 (6.83E-08)	9.92E-07 (9.64E-08)
DSU+2%DES	7.18E-07 (2.96E-08)	1.08E-06 (9.98E-08)

water in the hygroscopic PIL. Only after 400 m, once water has evaporated due to the temperature increase at the sliding contact [17], friction coefficient values reach those of the blends, after a severe surface damage on the steel surface has been produced.

In the same way, the friction and wear reduction ability observed for (DSU + DES) blends could also be attributed to several factors. In the first place, the ordered liquid crystalline phase present in DES additive, increases the viscosity and load-carrying ability of the lubricant. The long alkyl chain present in DES could contribute to a more effective interface separation. The formation of ordered ionic liquid films in confined environments have been previously shown by surface force apparatus (SFA) measurements [35].

A 1 wt% DES proportion added to DSU produces stable lubricant layers, which are not improved by the addition of a higher number of DES molecules in (DSU+2%DES). When compared with water-based lubricants, the use of (DSU + DES) blends prevents the solidification of the liquid crystalline DES additive in (Water + DES) and eliminates the need for evaporation of absorbed water to form a low friction boundary layer in (Water + DSU).

Fig. 10a shows that no wear scar, nor adhered material, are observed on the surface of the sapphire ball, after lubrication with neat DSU. In contrast, the stainless steel disk presents severe wear at the end of the tribological test (Fig. 10b) SEM micrograph (Fig. 10c) of the wear track on stainless steel surface shows plastic deformation at the edges and abrasion marks, parallel to sliding direction, inside the wear track. EDX carbon element map (Fig. 10d) shows that this element from the DSU lubricant is concentrated inside the wear track, particularly on the plastically deformed edges and on the abrasion marks.

After lubrication with (DSU+1%DES), the sapphire ball is, as expected, free from surface damage (Fig. 11a), as was previously observed for neat DSU (Fig. 10a). The photograph of the steel disk (Fig. 11b) after the tribological test shows that the lubricant appears transparent, in sharp contrast with the case of DSU (Fig. 10b).

SEM micrograph of the wear track on the steel disk (Fig. 11c) shows a mild wear without plastic deformation and with less abrasion marks than those observed for DSU. Carbon element map in Fig. 11d shows that there are no higher carbon concentration areas on the steel disk, as compared with DSU (Fig. 10d).

(DSU+2%DES) shows an intermediate behavior between those of DSU and (DSU+1%DES). The sapphire ball is again free from surface damage (Fig. 12a), but the wear track can be clearly observed on the surface of the steel disk after the test (Fig. 12b). SEM micrograph of the wear track (Fig. 12c) shows a more severe abrasion damage than that observed for (DSU+1%DES) (Fig. 11c), without the severe plastic
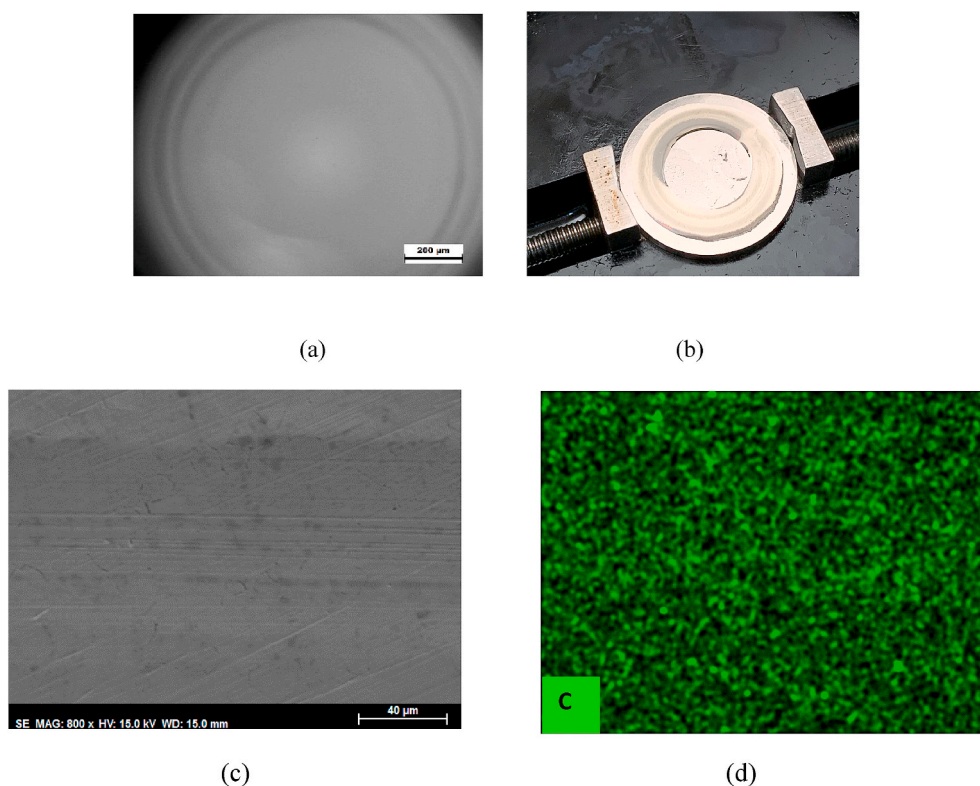
(a)

(b)

(c)

(d)

Fig. 11. Lubrication with (DSU+1%DES): a) Sapphire ball; b) Photograph of the AISI 316L disk after the test; c) SEM micrograph of wear track on AISI 316L steel disk; d) EDX carbon element map.

deformation observed for DSU (Fig. 10c), and without carbon increase on the sliding path (Fig. 12d).

Raman microscopy does not show the characteristic peaks of DSU or DES inside the wear tracks after lubrication tests. EDX spectra of steel disks after tribological tests with all lubricants show the characteristic peaks for stainless steel (Fig. 13), both inside and outside the wear track. In all cases, average iron, carbon and oxygen atomic percentages (± 1) are 61%, 9% and 2%, respectively. In order to elucidate the outer layer composition of the steel surface, it is necessary to complement these studies with XPS results.

XPS surface analysis of AISI 316L stainless steel after lubrication with DSU has been previously described [36]. XPS surface analysis results for steel disk surface after lubrication with (DSU+1%DES) are shown in Table 4. Both binding energy values and atomic percentages are similar inside and outside the wear track on stainless steel after lubrication with (DSU+1%DES), that is, the applied load at the sliding contact has not produced a significant change in the composition of the surface after the tribological test. C1s peaks in the range 286–288 eV are assignable to (C-N), (C-O) and (C=O), respectively. O1s signals at 530, 531 and 532 eV could be assigned to oxide, hydroxide and carboxylate, respectively. Two N1s peaks at 400 and 402 eV could be attributed to ammonium cations. Finally, the main iron peaks at 710 and 712 eV correspond to iron oxides and hydroxide, respectively. A minor peak at 707 eV is due to Fe (0) binding energy.

Although he above described post-tribo test surface analysis results cannot provide information about the situation at the initial running-in stage, they show that the chemical elements, both from anions and cations, present in the blend remain on the stainless steel surface after the test.

4. Conclusions

A fatty acid derived stearate protic ammonium ionic liquid crystal has been studied as 1 wt% and 2 wt% additive of a succinate protic ionic liquid, sharing a common 2-hydroxyethylammonium cation. The mesomorphic behavior of neat stearate ionic liquid crystal is also present in the lubricant blends, under static conditions before the tribological tests. The new lubricant blends are non-Newtonian fluids which increase steady state viscosity of the neat succinate base lubricant by a factor higher than four.

The main effect of the additive is the reduction of the running-in friction coefficient. Neat succinate ionic liquid shows a very high initial friction coefficient which is strongly reduced by the blends, with a reduction higher than 70% in the case of the blend containing 1 wt% additive. A wear rate reduction up to 95% with respect to the base lubricant is achieved by the new blends. The blend containing 1 wt% stearate ionic liquid crystal is the most effective lubricant, with the highest reduction of the running-in friction coefficient and the lowest surface damage.

The good tribological performance of the lubricant blends is attributed to the formation of adsorbed ordered layers with high load-carrying and surface protective abilities.

The results presented here confirm the feasibility of the use of ionic liquids and ionic liquid crystals derived from renewable resources both as lubricants and additives to obtain ionic liquid crystal blends with enhanced lubricant performance, yielding low running-in friction co-efficients, mild wear and absence of tribocorrosion.
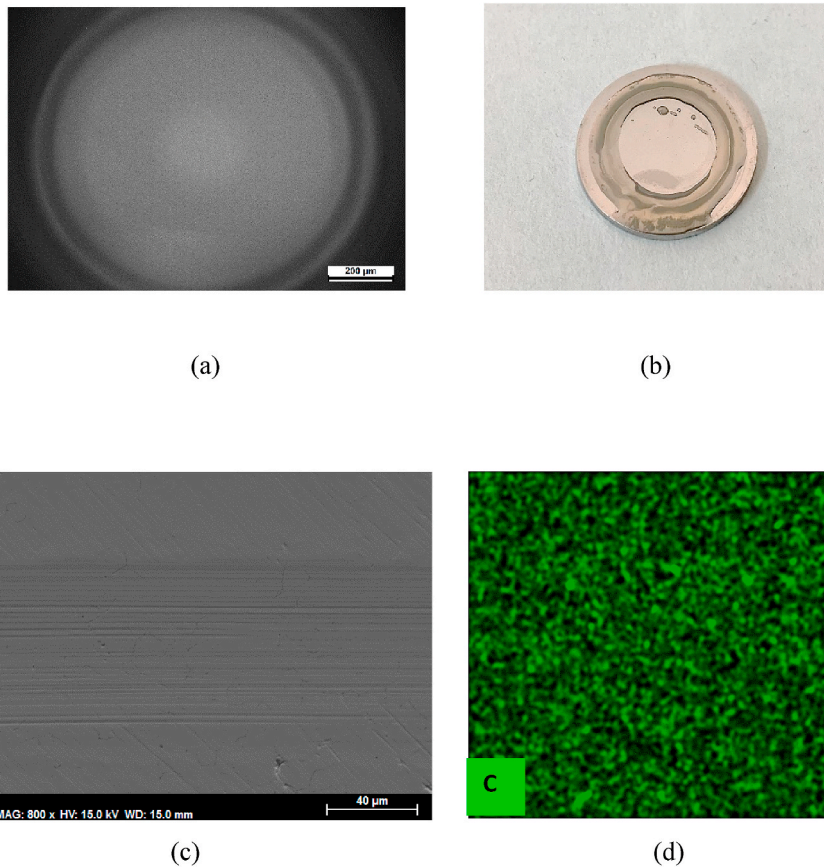
(a)

(b)

(c)

(d)

Fig. 12. Lubrication with (DSU+2%DES): a) Sapphire ball; b) Photograph of the AISI 316L disk after the test; c) SEM micrograph of wear track on AISIU 316L steel disk; d) EDX carbon element map.
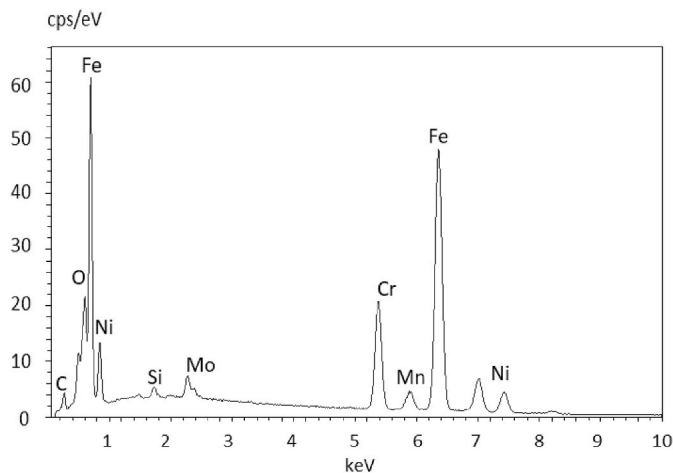

Fig. 13. EDX spectrum on AISI 316L stainless steel disk after a tribological test.

CRediT authorship contribution statement

M.D. Avilés: Investigation, Methodology, Software. **R. Pamies:** Investigation, Methodology, Software. **J. Sanes:** Methodology, Project administration, Funding acquisition. **J. Arias-Pardilla:** Investigation, Methodology, Software. **F.J. Carrión:** Methodology, Project administration, Funding acquisition. **M.D. Bermúdez:** Supervision, Writing - review & editing, Methodology, Project administration, Funding acquisition.

Table 4
XPS analysis results obtained inside and outside the wear track on stainless steel surface after lubrication with DSU+1%DES.

Element	Binding energy (eV) (atomic %)	
	Outside the wear track	Inside the wear track
C 1s	285.0 (17.9)	285.0 (17.4)
	286.0 (6.9)	285.7 (1.3)
	286.6 (8.6)	286.4 (13,6)
	288.4 (8.6)	288.4 (7.5)
O 1s	529.9 (17.1)	529.9 (19.9)
	531.3 (13.4)	531.3 (14.2)
	532.6 (15.2)	532.6 (12.7)
N 1s	400.1 (2.3)	400.2 (2.1)
	401.9 (0.9)	401.9 (0.7)
Fe 2p3/2	710.4 (4.2)	710.2 (3.6)
	712.3 (1.7)	711.9 (2.9)
	706.9 (0.6)	706.9 (0.7)

Declaration of competing interest

The authors declare that they have no known competing financial interests or personal relationships that could have appeared to influence the work reported in this paper.

Acknowledgments

References

[1] Ye C, Liu W, Chen Y, Yu L. Room-temperature ionic liquids: a novel versatile lubricant. Chem Commun 2001:2244–5.

[2] Bermúdez MD, Jiménez AE, Sanes J, Carrión FJ. Ionic liquids as advanced lubricant fluids. Molecules 2009;14:2888–908.

[3] Minami I. Ionic liquids in tribology. Molecules 2009;14:2888–908.

[4] Zhou Y, Qu J. Ionic liquids as lubricant additives: a review. ACS Appl Mater Interfaces 2017;9:3209–22.

[5] Torimoto T, Tsuda T, Okazaki K, Kubawata S. New frontiers in materials science opened by ionic liquids. Adv Mater 2010;22:1196–221.

[6] Zhou Y, Qu J. Ionic liquids as lubricant additives. ACS Appl Mater Interfaces 2017; 9:3209–22.

[7] Khemchandani B, Somers A, Howlett R, Jaiswal AK, Sayanna E, Forsyth MA. Biocompatible ionic liquid as an antiwear additive for biodegradable lubricants. Tribol Int 2014;77:171–7.

[8] Syahir AZ, Zulkitli NWM, Masjuki HH, Kalam MA, Alabdulkarem A, Gulzar M, Khong LS, Harith MH. A review on bio-based lubricants and their applications. J Clean Prod 2017;168:997–1016.

[9] Amiril SAS, Rahim EA, Syahrullail S. A review on ionic liquids as sustainable lubricants in manufacturing and engineering: recent research, performance and applications. J Clan Prod 2017;168:1571–89.

[10] Greaves TL, Drummond CJ. Protic ionic liquids: properties and applications. Chem Rev 2008;108:206–37.

[11] Zheng DD, Wang XB, Zhang M M, Ju C. Synergistic effects between the two choline-based ionic liquids as lubricant additives in glycerol aqueous solution. Tribol Lett 2019;67:47.

[12] Zheng DD, Zhao Q, Ju C, Wang XB. The interaction of two anticorrosive ionic liquid additives on the friction properties of water lubricants. Tribol Int 2020;141: 105948.

[13] Shi YJ, Larsson R. Non-corrosive and biomaterials protic ionic liquids with high lubricating performance. Tribol Lett 2016;63:1.

[14] Chan CH, Tang SW, Mohd NK, Lim WH, Yeong SK, Idris Z. Tribological behaviour of biolubricant base stocks and additives. Renew Sustain Energy Rev 2018;93: 145–57.

[15] Avilés MD, Cao VD, Sánchez C, Arias-Pardilla J, Carrión-Vilches FJ, Sanes J, Kjoniksen Al AL, Bermúdez MD, Pamies R. Effect of temperature on the rheological behavior of a new aqueous liquid crystal bio-lubricant. J Mol Liquids 2020;301: 112406.

[16] Avilés MD, Cao VD, Sánchez C, Arias-Pardilla J, Carrión-Vilches FJ, Sanes J, Kjoniksen AL, Bermúdez MD, Pamies R. Corrigendum to "Effect of temperature on the rheological behavior of a new aqueous liquid crystal bio-lubricant. J Mol Liq 2020;301:112406. J Mol Liquids 2020; 303:112645.

[17] Espinosa T, Jiménez M, Sanes J, Jiménez AE, Iglesias M, Bermúdez MD. Ultra-low friction with a protic ionic liquid boundary film at the water-lubricated sapphire-stainless steel interface. Tribol Lett 2014;53:1–9.

[18] Espinosa T, Sanes J, Jiménez AE, Bermúdez MD. Protic ammonium carboxylate ionic liquid lubricants of OFHC copper. Wear 2013;302. 495-509.9.

[19] Amzad K, Yasa SR, Gusain R, Khatri OP. Oil-miscible, halogen-free, and surface-active lauryl sulphate derived ionic liquids for enhancement of tribological properties. J Mol Liquids 2020;318:114005.

[20] Amzad K, Gusain R, Saha M, Khatri OP. Fatty acids-derived protic ionic liquids as lubricant additive to synthetic lube base oil for enhancement of tribological properties. J Mol Liquids 2019;293:111444.

[21] Fan MJ, Ma I, Zhang CY, Wang ZJ, Ruan JC, Han M, Ren YY, Zhang C, Yang DS, Zhou F, Liu WM. Biobased green lubricants: physicochemical, tribological and toxicological properties of fatty acid ionic liquids. Tribol Trans 2018;61:195–206.

[22] Alvarez VH, Dosil N, Gonzalez-Cabaleiro R, Mattedi S, Martin-Pastor M, Iglesias M, Navaza JM. Bronsted ionic liquids for sustainable processes; synthesis and physical properties. J Chem Eng Data 2010;55:625–32.

[23] Gusain R, Khatri OP. Fatty acid ionic liquids as environmentally friendly lubricants for low friction and wear. RSC Adv 2016;6:3462–9.

[24] Gusain R, Khan A, Khatri OP. Fatty acid-derived ionic liquids as renewable lubricant additives: effect of chain length and unsaturation. J Mol Liquids 2020; 301:112322.

[25] Toledo AAC, Maximo GJ, Costa MC, Cunha RI, Pereira JFB, Kurnia KA, Batista EAC, Meirelles AJA. Phase behaviour and physical properties of new biobased ionic liquid crystals. J Phys Chem B 2017;121:3177–89.

[26] Maximo GJ, Santos RJBN, Lopes-da-Silva JA, Costa MC, Meirelles AJA, Coutinho JAP. Lipidic protic ionic liquid crystals. ACS Sustainable Chem Eng 2014; 2:672–82.

[27] Carrión FJ, Avilés MD, Nakano K, Tadokoro C, Nagamine T, Bermúdez MD. Diprotic ammonium palmitate ionic liquid crystal and nanodiamonds in aqueous lubrication. Film thickness and influence of sliding speed. Wear 2019;418–419: 241–52. 2019.

[28] Avilés MD, Pamies R, Sanes J, Carrión FJ, Bermúdez MD. Fatty acid-derived ionic liquid lubricant, Protic ionic liquid additives. Coatings 2019;9:710.

[29] Avilés MD, Sánchez C, Pamies R, Sanes J, Bermúdez MD. Ionic liquid crystals in tribology. Lubricants 2019;7. Article Number 72.

[30] Avilés MD, Carrión FJ, Sanes J, Bermúdez MD. Effects of protic ionic liquid crystal additives on the water-lubricated sliding wear and friction of sapphire against stainless steel. Wear 2018;408–409:56–84.

[31] Wang Y, Wu Y, Yu Q, Zhang J, Ma Z, Zhang I, Zhang Y, Bai Y, Cai M, Feng Z, Liu W. Significantly reducing friction and wear of water-based fluids with shear thinning bicomponent supramolecular hydrogels. Adv Mater Interfaces 2020:2001084.

[32] Andrade RS, Torres D, Ribeiro FR, Chiari BG, Oshiro JA, Iglesias M. Sustainable cotton dying in non-aqueous medium applying protic ionic liquids. ACS Sustainable Chem Eng 2017;5(10):8756–65.

[33] Socrates G. Infrared and Raman characteristic group frequencies. third ed. J. Wiley & Sons Ltd.; 2001. 0470093072.

[34] Ba Z, Huang G, Qiao D, Feng D. Experimental and calculation studies on the relationship between the hygroscopic behaviour and lubrication properties of ionic liquids. Appl Surf Sci 2020;529:147031.

[35] Perkin S. Ionic liquids in confined geometries. Phys Chem Chem Phys 2012;14: 5052–62.

[36] Avilés MD, Carrion-Vilches FJ, Bermudez MD. Diprotic ammonium succinate ionic liquid in thin film aqueous lubrication and in graphene nanolubricant. Tribol Lett 2019;67:26.